Fiber optic detector probes for laser light scattering

Harbans S. Dhadwal, Chi Wu, and Benjamin Chu

An experimental investigation of the role of fiber optic detector probes in laser light scattering is presented. A quantitative comparison between different detector configurations is accomplished by measuring the time taken for one million photocounts to be accumulated in the extrapolated zeroth delay channel of the net unnormalized intensity time correlation function. A considerable reduction in the accumulation time is achieved by relaxing a rather stringent requirement for the spatial coherence of the optical field.

I. Introduction

In recent years there has been a considerable resurgence of interest in the use of optical fibers in laser light scattering (LLS).[1–5] The primary motivation is the possible miniaturization of the LLS apparatus as well as a capability of remote transmission and detection of laser light. LLS is concerned with an angular mapping of both the static and dynamic properties of the scattered laser light intensity. In an earlier paper[1] we presented the design of a fiber optic spectrometer which used fiber optic detector probes—each comprising an optical fiber and a Selfoc[6] graded index microlens. Spatial coherence requirements of the optical field translate into an effective entrance pupil and numerical aperture of a particular detector configuration. Design of an efficient fiber optic probe for dynamic light scattering (DLS) was discussed by Dhadwal and Chu.[1] In this paper, we investigate the properties of two particular fiber optic detector probes and compare their performance to a conventional detection geometry.

II. Theoretical Background

Optical mixing spectroscopic techniques in laser light scattering are well established for the study of dynamic properties of physical systems. The first order electric field time correlation function is directly measured using heterodyne mixing or indirectly via self-beating. The precision of the measured intensity time correlation function has been investigated by many workers.[7,8] Degiorgio and Lastovka[8] gave an in-depth generalized treatment of the precision of intensity time correlation functions for several experimental conditions. As discussed by them from a practical viewpoint one would like to achieve the highest possible measurement accuracy in the minimum amount of time. The ultimate limit is determined by statistical errors due to the finite measurement time.

For the case of a Gaussian optical field with an exponential intensity time correlation function, Degiorigio and Lastovka[8] expressed the precision of measurement by computing the ratio of the rms error to the amplitude of the signal term,

$$\Delta R(c) = \frac{\langle \delta R^2(0;c) \rangle^{1/2}}{c \langle n \rangle^2}, \tag{1}$$

where

$$\langle \delta R^2(0;c) \rangle = \frac{1}{N_s}(A + B + C),$$

$$A = \langle n \rangle^4 \left[-4c^3 - 6c^2 - 2c - 8 + \frac{8(c^3 + 2c^2 + c)}{1 - \exp\left(-\frac{\Delta\tau}{\tau_c}\right)} + \frac{4(c^2 + c)}{1 - \exp\left(-\frac{\Delta\tau}{\tau_c}\right)} \right]$$

$$B = \langle n \rangle^3 (4c^3 + 12c^2 + 8c),$$

$$C = \langle n \rangle^2 (c^2 + c),$$

$\langle \delta R^2(0;c) \rangle$ is the mean square deviation between the measured and expected intensity correlation function, $\langle n \rangle$ is the average number of photocounts in the time interval δt (which is often made equal to the delay time increment $\Delta\tau$) per single coherence area, c is the number of coherence areas as seen by the detector, $N_s (= T/\Delta\tau)$ is the total number of samples, T is the total duration time of the experiment, and τ_c is the correla-

All authors are with State University of New York at Stony Brook, Stony Brook, New York 11794. H. S. Dhadwal is in the Department of Electrical Engineering, C. Wu is in the Department of Chemistry, and B. Chu is in the Department of Materials Science & Engineering.

Received 11 October 1988.
0003-6935/89/194199-07$02.00/0.

tion time. Mandel and Wolf[9] gave an excellent treatment of the optical field coherence. The definition of the coherence area for a planar quasimonochromatic extended source can be found in that reference. In the derivation of Eq. (1) Degiorgio and Lastovka[8] have assumed that the coherence area is sufficiently large to ensure that there are no correlations among the currents arising from neighboring coherence areas. For the purpose of our paper we manipulate Eq. (1) to obtain an expression for the experiment duration time period T necessary to achieve a certain value for ΔR:

$$T = \frac{\Delta\tau}{\Delta R^2 c^2 \langle n\rangle^4}(A + B + C). \tag{2}$$

Figure 1 shows a plot of Eq. (2) as a function of $\langle n\rangle$ for various values of c. We have used our experimental values of $\Delta t = 25\ \mu$s, $\tau_c = 1.25\ 10^{-3}$ s, and $\Delta R = 10^{-3}$. From Fig. 1 we can easily conclude the well accepted result that for a single coherence area detector the accumulation time in the limit of $\langle n\rangle \to \infty$ is the shortest possible for any value of $\langle n\rangle$. However, another important conclusion can also be drawn from Fig. 1. In the region $\langle n\rangle$ less than unity it is quite possible to have a detector arrangement where the accumulation time can decrease with an increase in c. This situation arises because $\langle n\rangle$ is proportional to the photocount rate, which increases with increasing values of c. One such trajectory is that from a point A (c = 1 and $\langle n\rangle = 0.05$) to a point B ($c = 10$ and $\langle n\rangle = 0.1$). This transition is accompanied by a proportional decrease in the accumulation time. In a practical situation it is not possible to estimate with sufficient accuracy values of c and $\langle n\rangle$ so that a confident prediction of the expected improvement could be justified.

To make a meaningful comparison of the performance of each of the detectors let us recall that in photon correlation spectroscopy (PCS) the unnormalized intensity time correlation function is[10]

$$G^{(2)}(\tau) = \langle \mathbf{n}(t)\cdot\mathbf{n}(t+\tau)\rangle, \tag{3}$$

where τ is the delay time and $\mathbf{n}(t)$ [$\equiv c\langle\mathbf{n}(t)\rangle$] is the number of photocounts at time t in the time interval δt, $\langle\cdot\rangle$ denotes an ensemble average. For a self-beating experiment $G^{(2)}(\tau)$ can be related to the first order normalized electric field correlation function $g^{(1)}(\tau)$ by the Siegert relation[7]

$$G^{(2)}(\tau) = N_s\langle\mathbf{n}\rangle^2[1 + \beta|g^{(1)}(\tau)|^2], \tag{4}$$

where N_s is the total number of samples (or products), $\langle\mathbf{n}\rangle$ is the mean counts per sample time, and β is the so-called spatial coherence factor. β is in practice difficult to compute for a generalized 3-D quasimonochromatic spatially incoherent source. Consequently, it is invariably included as one of the parameters to be determined experimentally or in the analysis stage. Jakeman *et al.*[11] computed β for a very special configuration. $G^{(2)}(\tau)$ decays from an initial value of $N_s\langle\mathbf{n}^2\rangle$ to a baseline value of $N_s\langle\mathbf{n}\rangle^2$, which will be referred to as A. A real time measurement of the intensity correlation does not permit a continuous monitoring of the ratio of the rms to the signal amplitude, Eq. (1). However, as indicated in Eq. (1), ΔR is inversely proportional to the signal term. Thus, in practical situations, a quantitative comparison between different types of detector probe can be accomplished by defining two measurement times t_{base} and t_{net}. The former represents the time required to accumulate a given number of photocounts in the baseline channel, and the latter represents the time required to accumulate a net number of photocounts ($=A\beta$) in the extrapolated zeroth delay channel, that is, the signal term. These quantities can be defined from Eq. (4) as follows:

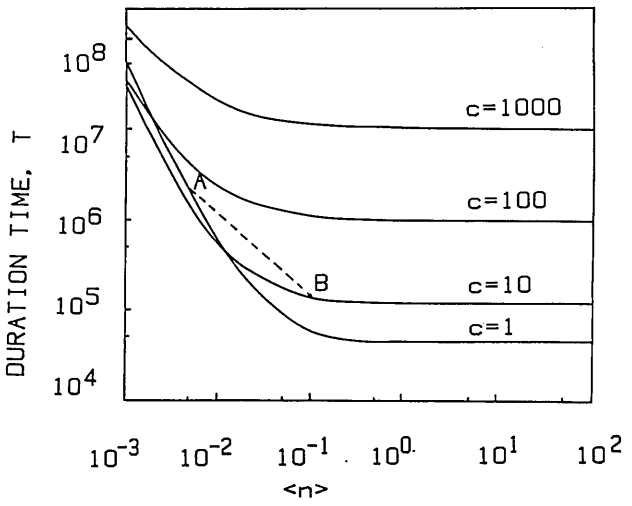

Fig. 1. Plot of the accumulation time T as a function of the counts per channel per single coherence area for various values of c, Eq. (2). $\tau_c = 1.25\ 10^{-5}$, $\Delta\tau = 25\ \mu$s, and $\Delta R = 10^{-3}$.

$$t_{\text{base}} = \frac{1}{\bar{n}^2}\frac{A}{\Delta\tau}, \tag{5}$$

where $\bar{n}$ is the mean count rate (counts per second), $\Delta\tau$ is the delay time increment, and $\langle\mathbf{n}\rangle$ has been replaced by $\bar{n}\Delta\tau$ and N_s by $T/(\Delta\tau)$. The function $g^{(1)}(\tau)$ in Eq. (4) has an initial value of unity and decays to zero at $\tau = \infty$. For the ideal case $\beta = 1$, the net unnormalized electric field correlation function has a value of A at $\tau = 0$. Thus the accumulation time t_{net} for a net count of A would be equal to t_{base}. For a finite value of β

$$t_{\text{net}} = \frac{t_{\text{base}}}{\beta}. \tag{6}$$

As expected Eq. (6) tells us that as $\beta \to 0$ $t_{\text{net}} \to \infty$. The performance of the various detectors is compared by computing t_{base} and t_{net} required to accumulate a baseline and a net photocount of say one million.

III. Description of the Detector Probes

A. Eyepiece Detector

The detector geometries for PCS systems have evolved over the years and consequently have become easier to align. One such system currently being employed was described by Chu and Wu.[12] A commercial eyepiece (manufactured by Gamma Scientific) together with a large optical fiber or a fiber bundle is used to provide a suitable detector arrangement as shown in

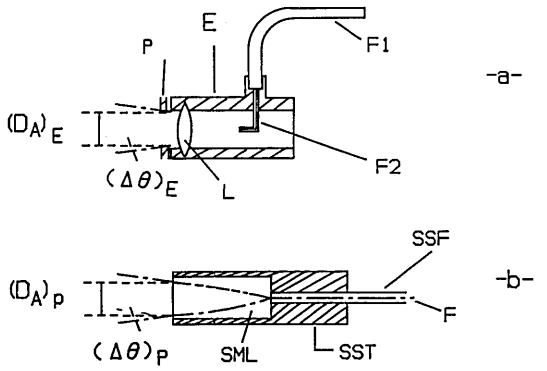

Fig. 2. Schematic of the various detector geometries. (a) Eyepiece detector: E, Gamma Scientific eyepiece; $F1$, 1.0-mm diam polymer optical fiber manufactured by Diaguide, Inc.; $F2$, fixed optical fiber of diameter D_{fe}; L, biconvex lens (f = 5 cm); P, pinhole of diameter D_P; $(D_A)_E$, length of scattering region; $(\Delta\theta)_E$ = 0.6 mrad. (b) Fiber optic detector probe: SST, machined piece of cylindrical stainless steel; SML, Selfoc microlens; SSF, stainless steel or ceramic ferrule;

$$(\Delta\theta)_p = \frac{D_f}{2} N_0\sqrt{\mathbf{A}}; \quad (D_A)_p = \frac{2(N.A.)_f}{N_0\sqrt{\mathbf{A}}}.$$

Fig. 2(a). The eyepiece has a biconvex lens which images the scattering volume onto the front end of an optical fiber permanently positioned in the image plane. The scattered light is extracted from the eyepiece by means of a second optical fiber. Note that the optical fibers used in the eyepiece detector are made of a single piece of glass (or polymer) and are not those used in lightwave communications. For this arrangement the divergence angle $(\Delta\theta)_E$ of the composite detector is controlled by means of a pinhole positioned in front of the lens, and the field of view is determined by the size of the fixed fiber and the lens magnification ratio. From Fig. 2(a) we find that $(\Delta\theta)_E$ and the effective diameter $(D_A)_E$ of the eyepiece detector are given by

$$(\Delta\theta)_E = \tan^{-1}\left(\frac{D_p}{2U}\right), \tag{7a}$$

$$(D_A)_E = \frac{1}{m} D_{fe}, \tag{7b}$$

where D_p is the diameter of the pinhole, U and V are the distances of the scattering center and fixed fiber from the lens, respectively; D_{fe} is the diameter of the fixed fiber, and m is the magnification of the imaging configuration. For our particular setup D_{fe} = 700 μm, D_p = 178 μm, $U = 2V$ = 15.5 cm giving $(\Delta\theta)_E$ = 0.6 mrad, and $(D_A)_E$ = 1.4 mm. The second fiber, which does not affect the performance of the eyepiece detector, was a 1-mm diam polymer fiber manufactured by Diaguide (SL/SG-1000 × 2m) and is used to extract light from the eyepiece and deliver it to a remotely located photomultiplier. However, the insertion loss into the 1-mm fiber introduced an ~50% intensity loss.

B. Fiber Optic Detector Probes

Our fiber optic detector probe is a compact receiver for collecting the scattered light from a quasimonochromatic 3-D extended source. To obtain an intensity time correlation function it is necessary for the receiver to satisfy certain spatial coherence requirements. These translate into an effective diameter and numerical aperture of the receiver. Thus the design step involves matching the available optical fibers and graded index microlenses so that the desired receiver characteristics are achieved. It should be noted that the role of the optical fiber is essentially that of a field stop with a well defined numerical aperture. Waveguiding properties of the optical fiber do not play a role in the design process. In addition, the optical fiber, serving as a light pipe, allows a photodetector to be located remotely. It should be noted that the optical fiber is essentially being used to transmit light from one end to the other end. Polarization states and modal mixing are not important. However, if the optical fiber were used as a receiver without the microlens, such factors as modal crosstalk and launch–loss become very important considerations. Indeed, attempts to control or specify the spatial coherence requirements at the exit end of the optical fiber are doomed to failure for these reasons.

The design of the fiber optic detector probes has been described elsewhere[1] and is not discussed here. Essentially, the probe comprises a special optical fiber, the type used in lightwave communications, and a Selfoc graded index microlens as shown in Fig. 2(b). For such a detector probe, the divergence angle in air $(\Delta\theta)_p$ and the effective aperture $(D_A)_p$ are given by

$$(D_A)_p = \frac{2(\text{N.A.})_f}{N_o\sqrt{\mathbf{A}}}, \tag{8a}$$

$$(\Delta\theta)_p = \frac{D_f}{2} N_o\sqrt{\mathbf{A}}, \tag{8b}$$

where D_f and $(\text{N.A.})_f$ are the core diameter and numerical aperture (in air) of the optical fiber, respectively. The microlens has a quadratic refractive index profile $n(r) = N_o[1 - (\mathbf{A}/2)r^2]$, where N_o is the refractive index on the optical axis and $\mathbf{A}$ is the refractive index gradient constant. Two fiber optic detector probes with different characteristics were made. The first, probe 1, used a single mode fiber of 4-μm core diameter (NSG single mode fiber) and a microlens (NSG SLN2.0). The second, probe 2, used a 10-μm core diam multimode fiber (General Fiber Optics 16-10) and a microlens (NSG SLW1.8). The two probes, 1 and 2, gave aperture diameters of 1.3 and 0.410 mm and a divergence angle (in air) of 0.3 and 5.0 mrad, respectively.

Two different probes were constructed to investigate the relationship between the experiment duration time and a relaxation of the spatial coherence requirements. Increasing the solid angle subtended by the source at the probe surface reduces the magnitude of the complex degree of coherence of the optical field incident at the probe surface but increases the count rate. In fact, a 2 order of magnitude increase in the

count rate for probe 2 is expected. Launch losses are not a consideration when using probes as receivers. All the light incident into the probe is focused onto the core of the optical fiber for collection. The only significant loss is due to Fresnel reflection, encountered in going from lens to fiber. This, however, would be the same for both probes. There may be an additional loss in count rate for the single mode probe because of the mismatch between the core diameter and diffraction limited spot size, which will be a little larger if significant aberrations are present. Using the currently available optics this cannot be avoided. However, by increasing the diameter of the microlens, at present not commercially available, the diffraction limited spot size can be made smaller than the core without affecting the probe characteristics.

Each probe is carefully constructed and tested. The optical fiber is first mounted into a stainless steel ferrule, cleaved, and polished before being actively aligned into the back focal plane of the microlens. The composite probe is very rugged. The diameter of the effective entrance pupil and the numerical aperture are measured by launching light into the other end of the optical fiber. Incorporation of a particular probe into a conventional spectrometer requires a simple alignment step.

IV. Experimental Results

A laser beam from a Spectra-Physics He–Ne laser (SP124B) was focused into an aqueous suspension of 0.176-μm nominal diameter latex spheres. The focused spot had a beam waist diameter of $\approx$168 μm. The concentration of the sample was $\approx 10^{-8}$ g/mliter. The same sample was used for all the measurements reported in this paper. Each detector probe described in the previous section was mounted on the rotation arm of a goniometer in a conventional laser light scattering spectrometer as shown in Fig. 3. In all cases the scattered light intensity was detected by the same photomultiplier (EMI 9863B/350), and electronic processing of the signal was identical. A Brookhaven Instruments full digital correlator (BI2030) was used to measure the intensity time correlation function. In addition, a Hewlett-Packard photon counter (5316A) was used to record the signal count rate.

Measurements of the intensity time correlation function $G^2(\tau)$ were made at several scattering angles for each detector probe described in Sec. I. Figure 4 shows a semilog plot of the net baseline normalized correlograms,

$$\left[\frac{G^{(2)}(\tau)}{A} - 1\right]$$

at a scattering angle of 60°. For this, and all other plots in this paper, triangles, squares, and diamonds represent measurements made with the eyepiece detector and fiber optic detector probes 1 and 2, respectively. The intercept of the ordinate axis in Fig. 4 indicates the value of β, which as expected is the largest for the single mode fiber optic detector probe. The parallelism of the lines indicates very good agreement between the three data sets.

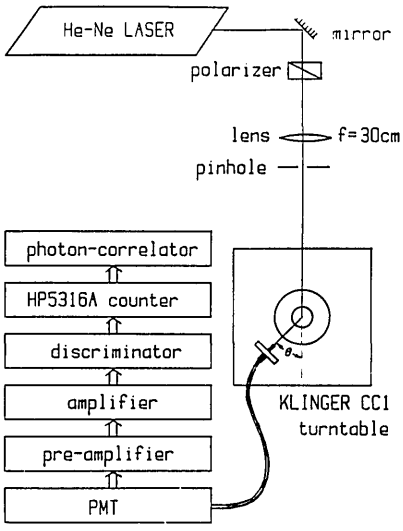

Fig. 3. Schematic layout of the optical spectrometer used to obtain the intensity–intensity time correlation functions. θ is the scattering angle.

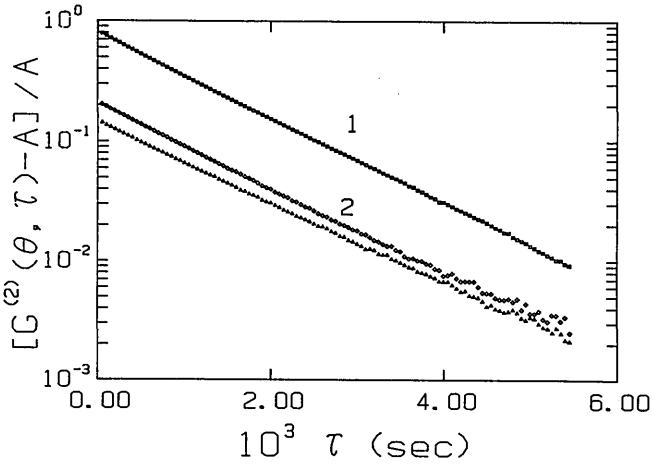

Fig. 4. Semilog plot of the net baseline normalized intensity–intensity time correlation function at a scattering angle of 60°. τ is the delay time. In this and subsequent figures triangles, squares, and diamonds correspond to measurements made with the eyepiece, probe 1, and probe 2, respectively.

To obtain a quantitative assessment of the accuracy of the measurements each data set was analyzed using an established nonlinear least squares curve fitting procedure based on the method of cumulants.[13] The function $g^{(1)}(\tau)$ in Eq. (4) can be related to the normalized linewidth distribution function $G(\Gamma)$ by a Laplace transform

$$g^{(1)}(\tau) = \int_{\Gamma_{min}}^{\Gamma_{max}} G(\Gamma) \exp(-\Gamma\tau) d\Gamma, \tag{9}$$

where $G(\Gamma) = 0$ for $\Gamma \geq \Gamma_{max}$ and $\Gamma \leq \Gamma_{min}$. The curve fitting procedure gives values of β, $\bar{\Gamma}$, and $\mu_2/\bar{\Gamma}^2$, with

$$\bar{\Gamma} = \int_{\Gamma_{min}}^{\Gamma_{max}} \Gamma G(\Gamma) d\Gamma, \tag{10a}$$

$$\mu_2 = \int_{\Gamma_{min}}^{\Gamma_{max}} (\Gamma - \bar{\Gamma})^2 G(\Gamma) d\Gamma. \tag{10b}$$

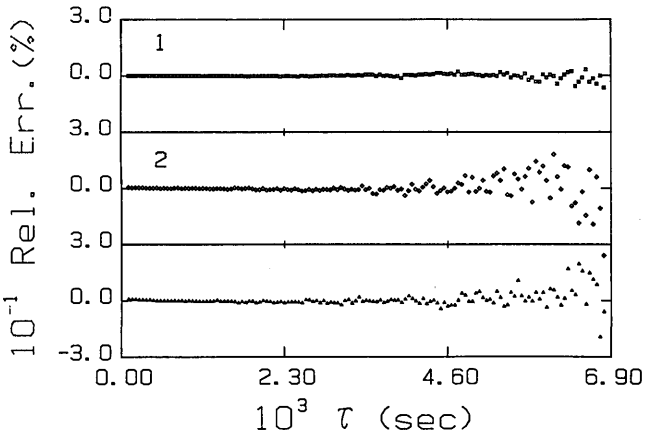

Fig. 5. Plot of the percentage relative deviations obtained from a nonlinear least squares fit to the data shown in Fig. 3:

$$\text{rel. err.} = \left\{\frac{[G^{(2)}(\tau)]_{\text{meas.}}}{[G^{(2)}(\tau)]_{\text{cal.}}} - 1\right\} \times 100.$$

The goodness of the curve fitting procedure is usually assessed by plotting the percentage relative deviations between the measured data and the result of fitting. Figure 5 shows a comparison between a typical set of deviation plots obtained for measurements made at 60° using each of the three detector probes. Table I shows a summary of the results obtained by analyzing all the data sets. From Table I we can ascertain that values of $\bar{\Gamma}$ agree to within 5% for measurements made with each probe. In addition, all the fits indicate a monodisperse system as expected.

Table I. Results of Nonlinear Least Squares Curve Fitting to the Net Baseline Normalized Intensity–Intensity Time Correlation Functions $\{[G^{(2)}(\tau)]/A\} - 1$ Measured from an Aqueous Suspension of 0.176-μm Nominal diam Latex Spheres (Concentration ≈ 10^{-8} g/milter)

θ	$\bar{\Gamma}$			$\frac{\mu_2}{\bar{\Gamma}^2}$		
	eyepiece	probe 1	probe 2	eyepiece	probe 1	probe 2
30	104	106	103	0.140	0.000	0.002
35	127	148	141	0.002	0.022	0.001
40	173	180	193	0.058	0.000	0.039
45	227	237	244	0.001	0.001	0.001
50	268	296	297	0.001	0.032	0.002
60	393	413	413	0.023	0.001	0.002
75	587	608	625	0.000	0.001	0.016
90	769	790	797	0.000	0.000	0.001
120	1030	1022	1098	0.059	0.024	0.023
145	1140	1101	1203	0.059	0.120	0.037

$\bar{\Gamma} = \int_{\Gamma_{\min}}^{\Gamma_{\max}} \Gamma G(\Gamma) d\Gamma$ and $\mu_2 = \int_{\Gamma_{\min}}^{\Gamma_{\max}} (\Gamma - \bar{\Gamma})^2 G(\Gamma) d\Gamma$. θ is the scattering angle in degrees; eyepiece refers to conventional detection geometry described in section II.A; probe 1 and probe 2 are described in section II.B.

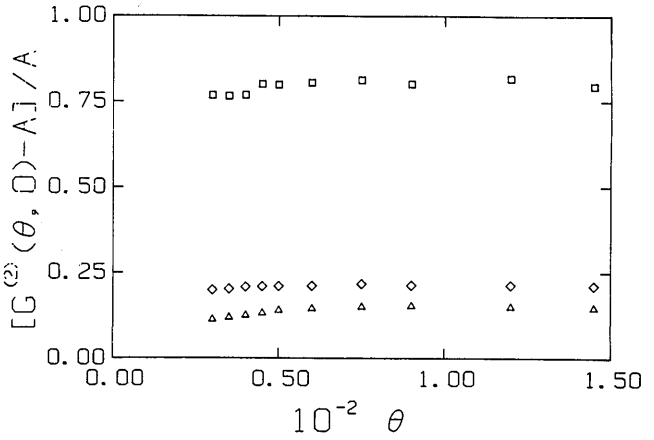

Fig. 6. Plot of the spatial coherence factor

$$\beta\left[= \frac{G^{(2)}(0)}{A} - 1\right]$$

as a function of the scattering angle for the three detector geometries described in Sec. I.

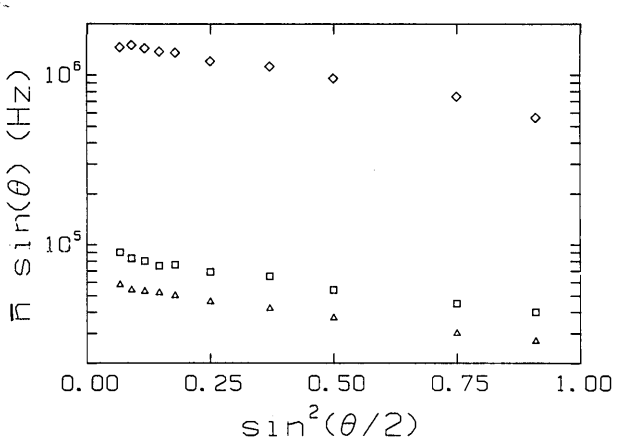

Fig. 7. Normalized signal count rate $\bar{n}\sin(\theta)$ vs $\sin^2(\theta/2)$ for the various detector probes.

From Eq. (4) we note that the spatial coherence factor β should be made as large as possible to increase the contributions due to the signal term. Figure 6 shows a plot of

$$\beta\left[= \frac{G^2(0)}{A} - 1\right]$$

for various scattering angles. All detector probes have a similar dependence on the scattering angle, but the single mode detector probe gives higher values of β. As pointed out earlier the mean signal count rate is also an important parameter. Figure 7 shows a plot of $\bar{n}\sin(\theta)$ vs $\sin^2(\theta/2)$ with θ being the scattering angle. We now note that the mean signal count rate for probe 2 is ≈100 times greater than probe 1. From the two plots in Figs. 6 and 7 one might conclude incorrectly that probe 1 is more suitable for DLS, whereas probe 2 may be better suited for static measurements of the scattered light intensity. However, as discussed in Sec. I the more prudent parameters of performance

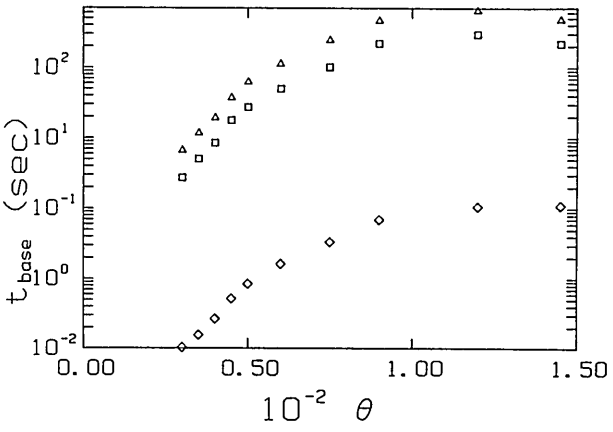

Fig. 8. Accumulation time

$$t_{base}\left(=\frac{A}{\bar{n}^2\Delta\tau}\right)$$

required to achieve a baseline count A of one million. $\bar{n}$ is the mean signal count rate (counts per second), $\Delta\tau$ is the delay time increment.

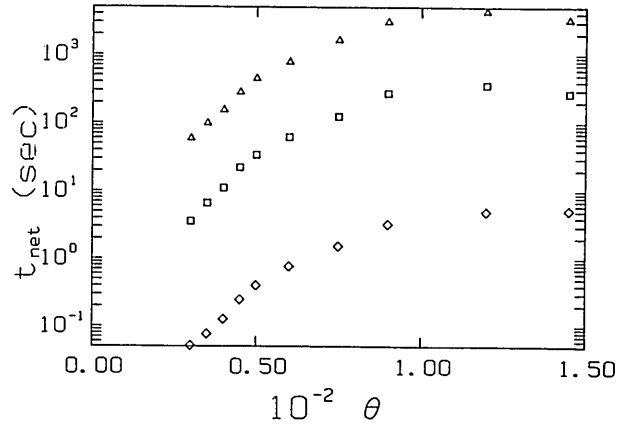

Fig. 9. Accumulation time

$$t_{net}\left(=\frac{t_{base}}{\beta}\right)$$

required to achieve a net count of one million. β is the spatial coherence factor defined in Eq. (4).

characterization are t_{base} and t_{net}. Figures 8 and 9 show plots of t_{base} and t_{net}, respectively. These accumulation times are computed for a baseline and a net photocount of one million. Note that these may be compared with the actual measurement times associated with the Brookhaven digital correlator used here. A factor of 16 has been included in the computations since the Brookhaven correlator has an internal scaling factor of 16. From Figs. 8 and 9 it is clear that probe 2 is the best choice for both static and dynamic measurements of the scattered light intensity. It should also be noted that for the eyepiece an additional gain factor of 4 is possible if the insertion loss into the 1-mm fiber is improved by better alignment.

V. Comments on the Use of Optical Fibers

The overriding design constraint in the development of detector probes suitable for DLS is that of meeting the spatial coherence requirements of the optical field. The spatial coherence requirements specify an effective entrance pupil diameter and numerical aperture for a generalized detector probe. It is of no consequence how this is achieved. Indeed conventional detector geometries using lenses and apertures have been successfully employed. The introduction of optical fibers and graded index microlenses has resulted in considerable miniaturization of the detector probes as well as of the whole light scattering spectrometer.[1] The role played by an optical fiber in our probe is essentially that of a field stop with a well defined numerical aperture. The former defines the angular uncertainty of the probe while the latter defines the diameter of the effective entrance pupil. Single mode fibers of the type used in communications were used primarily because of their small core diameters and not because of their waveguiding properties. The multimode fiber used in probe 2 has a core diameter of 10 μm and is in fact single mode at a wavelength of ~1.3 μm. Larger multimode fibers of 50-μm core diameter were found unsuitable for DLS,[1] because the resulting receiver was viewing a source which is almost spatially incoherent.

Finally, the measurements reported here were not concerned with polarization effects. If polarization is an important consideration, a suitable analyzer must be used in front of the fiber optic probe. Single mode polarization maintaining fiber is not recommended because of the considerable practical difficulties. Intermodal (multipath) and intramodal (chromatic) dispersions are not significant for fiber optic detector receivers. Microphony in the 10-μm optical fiber was not prevalent.

VI. Summary

In this paper we have quantitatively shown the important role that fiber optic/microlens detector probes will play in future LLS systems. The probe is no more than 2.0 mm in diameter and has a typical length of 15 mm. With existing choices of fiber diameters and microlens configurations the multimode fiber optic detector probe is a better choice than the single mode fiber optic detector probe.

Some of the results reported in this paper were presented at the NASA Laser Light Scattering Advanced Technology Workshop, 7–8 Sept. 1988, Cleveland, OH. H. S. D. and B. C. wish to acknowledge the support of a grant from NASA Lewis Research Center under contract NAG3963 and from the Polymers Program, National Science Foundation (DMR8617820), respectively.

Benjamin Chu also works in the Department of Chemistry.

References

1. H. S. Dhadwal and B. Chu, "A Fiber Optic Light Scattering Spectrometer," Rev. Sci. Instrum. **60**, 845–853 (1989).

2. H. Auweter and D. Horn, "Fiber-Optical Quasi-Elastic Light Scattering of Concentrated Dispersions," J. Colloid Interface Sci. **105**, 399–409 (1985).
3. R. G. W. Brown, "Dynamic Light Scattering Using Monomode Optical Fibers," Appl. Opt. **26**, 4846–4849 (1987).
4. R. G. W. Brown and A. P. Jackson, "Monomode Fibre Components For Dynamic Light Scattering," J. Phys. E **20**, 1503–1507 (1987).
5. H. S. Dhadwal and B. Chu, "Fiber Optics in Laser Light Scattering Spectroscopy," J. Colloid Interface Sci. **115**, 561–563 (1987).
6. Selfoc, trademark of NSG America, Inc., 28 Worlds Fair Dr., Somerset, NJ 08873.
7. H. Z. Cummins and H. L. Swinney, "The Theory of Light Beating Spectroscopy," Prog. Opt. **8**, 135–200 (1970).
8. V. Degiorgio and J. B. Lastovka, "Intensity Correlation Spectroscopy," Phys. Rev. A **4**, 2033–2050 (1971).
9. L. Mandel and E. Wolf, "Coherence Properties of Optical Fields," Rev. Mod. Phys. **37**, 231–287 (1965).
10. B. Chu, J. R. Ford, and H. S. Dhadwal, "Correlation Function Profile Analysis," in *Methods of Enzymology, Vol 117*, S. Collowick and N. O. Kaplan, Eds. (Academic, Orlando, FL, 1985).
11. E. Jakeman, C. J. Oliver, and E. R. Pike, "The Effects of Spatial Coherence on Intensity Fluctuation Distributions of Gaussian Light," J. Appl. Phys. **A5**, L45–L48 (1970).
12. B. Chu and C. Wu, "Light Scattering Characterization of an Alternating Copolymer of Ethylene and Tetrafluoroethylene," Macromolecules **19**, 1285–1286 (1986); **20**, 93–98 (1987).
13. D. E. Koppel, "Analysis of Macromolecular Polydispersity in Intensity Correlation Spectroscopy: The Method of Cumulants," J. Chem. Phys. **57**, 4814–4820 (1972).
